Epistatic networks jointly influence phenotypes related to metabolic disease and gene expression in Diversity Outbred mice

Anna L. Tyler, Bo Ji, Daniel M. Gatti, Steven C. Munger, Gary A. Churchill, Karen L. Svenson, Gregory W. Carter*

Anna.Tyler@jax.org
Bo.Ji@jax.org
Dan.Gatti@jax.org
Steven.Munger@jax.org
Gary.Churchill@jax.org
Karen.Svenson@jax.org
Gregory.Carter@jax.org

*Corresponding author: Gregory W. Carter
The Jackson Laboratory, 600 Main St, Bar Harbor, ME, USA

Abstract

Multiple genetic and environmental factors contribute to metabolic disease, with effects that range across molecular, organ, and whole-organism levels. Dissecting this multi-scale complexity requires systems genetics approaches to infer polygenic networks that influence gene expression, serum biomarkers, and physiological measures. In recent years, multi-parent model organism crosses, such as the Diversity Outbred (DO) mice, have emerged as a powerful platform for such systems approaches. The DO mice harbor extensive phenotypic and genetic diversity, allowing for detection of multiple quantitative trait loci (QTL) and their interactions at high genomic resolution. In this study, we used 474 DO mice to model genetic interactions influencing hepatic transcriptome expression and physiological traits related to metabolic disease. Body composition, serum biomarker, and liver transcriptome data from mice fed either a high-fat or standard chow diet were combined and simultaneously modeled. Modules of co-expressed transcripts were identified with weighted gene co-expression network analysis, with summary module phenotypes representing coordinated transcriptional programs linked to specific biological functions. We then used the Combined Analysis of Pleiotropy and Epistasis (CAPE) to simultaneously detect directed epistatic interactions between haplotype-specific QTL for transcript modules and physiological phenotypes. By combining information across multiple phenotypic levels, we identified networks of QTL with numerous interactions that reveal how genetic architecture affects metabolic traits at multiple scales. Specifically, these networks model how gene regulatory programs from different inbred founder strains influence more complex physiological traits. By connecting three levels of the organismal hierarchy – genetic variation, transcript abundance, and physiology – we revealed a detailed picture of genetic interactions influencing complex traits through differential gene expression.

Introduction

Traits relevant to metabolic disease, such as obesity, and blood lipid profiles, have complex genetic architecture (Schork 1997). Many genetic factors contribute to these traits and potentially interact to influence multiple traits simultaneously. Identifying these genes and their interactions will play a critical role in predicting individual susceptibility to metabolic disease and prioritizing drug targets for targeted treatments (Moore and Williams 2009). However, despite availability of large-scale genotype and phenotype data in multiple human populations, little is known about the genetic architecture of metabolic disease-related traits.

There are a number of challenges associated with mapping the genetic architecture of complex traits in human populations. In contrast to Mendelian traits, in which a single genetic variant is responsible for the vast majority of phenotypic variation, complex traits are influenced by many variants with small effects, which are difficult to detect. Large variation in environmental exposures between individuals can easily overwhelm small genetic effects, compounding the problem. Human populations, moreover, have intricate population structure (Rosenberg *et al.* 2002) which can cause spurious associations in genetic mapping experiments (Pritchard *et al.* 2000). Detecting genetic interactions, or epistasis, in humans raises additional challenges. Epistatic interactions tend to be weaker than main effects and can generate additive genetic variance (Huang and Mackay 2016), and variation in allele frequencies between populations makes replication of true interactions between populations difficult (Greene *et al.* 2009).

Highly diverse multi-parent populations, such as the Diversity Outbred (DO) mice (Svenson *et al.* 2012) [@Gatti] offer a powerful alternative to human populations for mapping the genetic architecture of complex traits. As an outbred population, the DO mice are potentially a better model of human populations than inbred mice. Because the DO founders included three strains recently derived from wild mice, the population contains extensive allelic variation that is evenly distributed

across the genome (Philip *et al.* 2011; Svenson *et al.* 2012; Logan *et al.* 2013). This density of polymorphisms allows much more extensive mapping than can be done in typical crosses between inbred strains, which can share large regions of identical sequence (Yang *et al.* 2011). Furthermore, the breeding paradigm in the DO is designed to maintain allelic diversity, reduce linkage disequilibrium, and generate minimal population structure (Svenson *et al.* 2012; Chesler *et al.* 2016). Thus variation in allele frequency does not confound detection of variant effects or epistasis as it does in human populations, and effects can be mapped to relatively narrow genomic loci, which will enhance the discovery of genetic influences on phenotype.

A large number of traits, including many clinically relevant traits, have been measured in DO mice (Svenson *et al.* 2012; Bogue *et al.* 2015) [and @Gatti]. While heritable, few of these traits have a single QTL of exceptional effect [@Gatti]. The DO mice thus provide an ideal platform for investigating the genetic architecture of complex traits. Their phenotypic diversity combined with extensive genetic variation that is evenly distributed and highly recombined facilitates detection of both genetic main effects and interactions influencing many clinically relevant traits.

In this study we use combined analysis of pleiotropy and epistasis (CAPE) {tyler2013cape} to investigate the genetic architecture of multiple complex traits related to metabolic disease in 474 male and female DO mice fed either a high-fat or standard chow diet. Specifically, we analyzed epistasis influencing fat mass, lean mass, and circulating levels of cholesterol, triglycerides, and leptin, as well as three gene expression phenotypes. CAPE is an approach that combines information across multiple phenotypes to infer directed genetic interactions. It infers a single model for multiple quantitative traits, and leverages statistical power from multiple phenotypes to enhance the detection of QTL and their interactions. With this approach, we recently analyzed the genetic architecture of body composition and bone density in a well-powered F_2 mouse intercross (Tyler *et al.* 2016) that revealed a large network of weak interactions that generally reduced phenotypic variation across the population. Here we apply the principles of this analysis to investigate the contributions of within-strain and between-strain epistatic interactions in the DO, augmented by interactive roles of sex and high-fat diet in the network.

Results

Transcripts with *trans* genetic effects cluster into functionally enriched modules

Because we were interested in genetic interactions that influence expression traits, which must include at least one *trans* effect, we first filtered the liver transcriptome to 3635 transcripts that were influenced by
trans genetic loci (Methods). We performed weighted gene correlation network
analysis (WGCNA) (Langfelder and Horvath 2008) on these transcripts and obtained 11 distinct modules. Using the Database for Annotation, Visualization and Integrated Discovery (DAVID) (Huang *et al.* 2009a; b) we found that three of these modules had significantly enriched functional annotations (Benjamini-adjusted $p \leq 0.05$): (1) cellular metabolic process (Metabolism Module)($p = 6.3 \times 10^{-17}$), (2) oxidation reduction process (Redox Module) ($p = 7.7 \times 10^{-7}$), and (3) immune response (Immune Module)($p = 5.2 \times 10^{-15}$) (Table 1). We used the module eigengenes from these modules as phenotypes for CAPE analysis (Methods) (Ghazalpour *et al.* 2006; Philip *et al.* 2014). We refer to them hereafter by their functional annotations.

Pleiotropic QTL influence physiological and expression traits

We combined the module eigengenes described above with five physiological traits: lean tissue mass, fat tissue mass, as well as cholesterol, leptin, and triglyceride levels. Fat mass was log-transformed to reproduce a more linear relationship with lean mass (Forbes 1987). These traits were modestly

correlated (Figure 1), implying that some genetic factors may be shared among the traits, while others may be distinct. To determine whether the traits here were influenced both by pleiotropic loci and loci specific to individual traits, we performed linear regression to associate the haplotype at each locus with each of our eight phenotypes (Methods). Across all traits, only one QTL for cholesterol on distal Chr 1 reached genome-wide significance (permutation-based $p < 0.05$). However, there were multiple loci where individual haplotypes had substantial effects that potentially contribute to polygenic etiology (Figure 2). In some cases, a single haplotype had an apparent effect on a single phenotype. For example, a positive effect of the NZO haplotype on cholesterol can be seen on distal Chr 11 (Figure 2). Likewise, the A/J haplotype at a nearby locus had a positive effect on leptin levels (Figure 2). Other loci were pleiotropic. The CAST haplotype at a third locus on chromosome 11 had negative effects on fat mass, cholesterol, leptin, triglycerides, and the Immune Module (Figure 2). This effect was shared to a lesser extent by the PWK haplotype in fat mass, leptin, and triglyceride levels. This complex pattern of effects suggests a complex underlying genetic architecture. The haplotype effects that are common across multiple phenotypes may represent a common genetic factor influencing multiple traits. We combined these common signals to gain information about individual loci. Haplotypes that influence a single phenotype, for example the NZO haplotype effect on cholesterol, provide non-redundant information that can be used to identify genetic factors with specific phenotypic effects.

Singular value decomposition concentrates functional genetic effects

We decomposed the trait matrix using singular value decomposition to obtain *eigentraits* (ETs) (Figure 3A). In our analysis we used the first three ETs, which captured 88.3% of the overall variance. ETs recombine covarying elements of the measured traits, and potentially concentrate functionally related effects. For example, leptin, cholesterol, and fat mass, along with the Redox and Immune Modules, were averaged in ET2. This ET appears to capture the CAST/PWK effect on Chr 11 noted early to influence multiple traits. (Figure 3B).

An epistatic network involving all haplotypes influences physiological and expression traits

Because there were more markers genotyped than could be tested exhaustively in pairs, we used a subset of haplotypes with the greatest effect-sizes in all three ETs (see Methods). The haplotype with greatest standardized effect from each potential QTL peak was retained and the peak was further sampled to keep 10% of markers within it. This process yielded a total of 515 markers representing all seven haplotypes on 17 chromosomes (The C57BL/6J haplotype was excluded because we used it as the reference strain). Because marker selection was based on effect size, the haplotypes were unevenly represented (Figure 5A). A/J was the most highly represented haplotype with 100 markers on eight chromosomes, and NOD was the least represented with 32. WSB alleles were the most widely distributed, being selected from 12 different chromosomes. We ran CAPE on these markers and the first three ETs to find an epistatic network between loci (Methods).

The resulting network consisted of 89 interactions among 49 loci and two covariates (Figure 4). All haplotypes participated in at least one interaction (Figure 5A). WSB haplotypes were involved in the largest number of interactions (32), while NZO participated in the fewest (8). The number of total interactions each haplotype participated in did not correlate with its representation in the 515 markers selected for the CAPE pipeline (Figure 5A) ($p = 0.1$). The final epistatic network was directed, meaning that interactions model a source marker that acts on a target marker, and we can thus measure the number of times each haplotype was the source of an interaction or the target of an interaction. The majority of haplotypes were roughly evenly represented as both sources and targets. However, the 129 haplotype was a target of interactions about four times more frequently than it was a source, while the NZO haplotype was a source about twice as many times as it was a target

(Figure 5A). The covariates, sex and diet were both much more frequently sources of interactions than they were targets (Figure 5A).

The interactions between haplotypes were most often between strains rather than within-strain (Figure 5B). Inter-strain interactions were concentrated among the 129, WSB, NZO and A/J haplotypes, which are all in the *Mus musculus domesticus* subspecies. CAST, *M. musculus castaneus*, interacted with each of the other strains relatively evenly, while PWK, *M. musculus musculus*, was the most isolated strain, and did not interact at all with the NZO or NOD haplotypes. The only haplotype with multiple intra-strain interactions was WSB. This may be due to the wide sampling of the selected WSB alleles from 12 different chromosomes resulting in more unique loci with potential for interacting with each other.

Sex interacted with all founder haplotypes

Sex significantly affected all physiological traits except leptin levels. This effect was positive for all phenotypes meaning that males had higher log fat mass (males 1.9 g, females: 1.7 g, $p = 5.7 \times 10^{-2}$), lean mass (males: 25.1 g, females: 18.3 g, $p < 2 \times 10^{-16}$), cholesterol (males 110.4 mg/dl, females: 93.8 mg/dl, $p = 4.3 \times 10^{-10}$), and triglycerides (males: 156.0 mg/dl, females: 115.0 mg/dl, $p = 7.6 \times 10^{-14}$). All expression modules were significantly lower in males (all $p < 2 \times 10^{-16}$). Sex also participated in interactions with genetic loci. The majority of genetic interactions with sex (12 of 15) involved a suppression of allele effects by sex, indicating that the alleles had larger effects in females than in males. Alleles from all founder strains were affected. One locus, the CAST allele on Chr 11, enhanced the effects of sex. The allele overall had negative effects on leptin, cholesterol, and lean mass, but in males, these measures were higher in the presence of this allele than expected from the additive model. There was also a single locus, the WSB allele on Chr 17, that suppressed the effects of sex, indicating that males carrying this allele had lower than expected lean mass, fat mass, etc. For example, both this allele and sex had positive effects on cholesterol, but cholesterol levels in male mice carrying this WSB allele were lower than expected from the additive model. Finally, phenotypic effects of the male sex were enhanced by the high-fat diet, suggesting that males were more susceptible to the effects of the high-fat diet.

Diet interacted with a subset of parental haplotypes

Diet significantly increased log fat mass (chow: 1.6 g, HF: 2.1 g, $p < 2 \times 10^{-16}$), cholesterol (chow: 85.8 mg/dl, HF: 119.1 mg/dl, $p < 2 \times 10^{-16}$), and leptin (chow: 7.7 mg/dl, HF: 19.7 mg/dl, $p < 2 \times 10^{-16}$) and significantly decreased triglyceride levels (chow: 146.7 mg/dl, HF: 124. 3 mg/dl, $p = 1 \times 10^{-4}$). It also significantly decreased all expression modules (all $p < 0.001$). Similar to sex, the majority of genetic interactions with diet (five of seven) were those in which high-fat diet suppressed genetic effects. That is, the alleles had greater phenotypic effect in chow-fed mice than mice on the high-fat diet. There was one locus, the CAST allele on Chr 2, that enhanced the effects of diet, indicating that animals carrying this allele were more susceptible to the effects of the high-fat diet. The effects of diet were also enhanced by sex, as mentioned above, indicating that males in this population were more susceptible to the effects of the high-fat diet than females.

Network motifs had both redundant and synergistic effects on phenotypes

To better understand the overall influence of genetic interactions on traits, we performed a network motif analysis as described in (Tyler *et al.* 2016). Network motifs are composed of one interaction between two loci, each of which has a main effect on one phenotype (Figure 6A). The interaction can either be suppressing or enhancing, and the two main effects can drive the phenotype either in the same direction (coherent) or in opposing directions (incoherent). Here we investigated the effects of

network motifs on traits in the DO and compare our results to our previous results from results from an F_2 intercross between inbred strains in Tyler et al. (2016) (Tyler *et al.* 2016).

Only enhancing-incoherent and suppressing-coherent motifs were present in the DO epistatic network (Figure 6B). They involved all parental haplotypes and were predominantly interactions between haplotypes from different parents (enhancing-incoherent: 72% different parental haplotypes, suppressing-coherent: 96% different parental haplotypes). In contrast to the intercross, the enhancing-incoherent motifs were not predominantly balancing, but tended to drive traits away from the population mean. The vast majority of these motifs (92%) had a destabilizing effect on phenotype, and 80% drove the phenotype past any additive prediction (Figure 7). A substantial fraction of the suppressing-coherent motifs (25%) were non-redundant, meaning they pushed phenotypes farther from the population mean than predicted by the additive model (Figure 7).

Discussion

Traits associated with metabolic disease, such as cholesterol levels, body fat mass, and triglyceride levels have complex genetic architecture. Mapping genes influencing these traits will help identify mechanistic factors influencing them and, together with molecular biomarkers, may ultimately provide targets for therapies. Mapping complex genetic effects, however, is challenging, especially in human populations in which environmental factors and population structure can overwhelm weak genetic effects. Mice offer an excellent alternative as pre-clinical model organisms in which to dissect complex traits mechanistically. However, the majority of inbred strains used in medical research are closely related to each other. The have limited phenotypic diversity and large genetic blind spots due to a lack of genetic variants between them. The DO mice provide a powerful alternative platform for fine-mapping complex traits. They harbor immense genetic and phenotypic diversity, and have minimal population structure, thereby allowing much more detailed assessments of complex genetic architecture influencing complex traits. The genetic diversity in the DO does create its own issues, however, in that large genetic effects can be difficult to find. Using standard mapping methods, we and others have shown that most traits are influenced by many QTL with small effects (@gatti), and few QTL rise to genome-wide significance. Here we used Combined Analysis of Pleiotropy and Epistasis (CAPE) to combine multi-dimensional phenotype information and test for genetic interactions influencing a suite of related traits. We found numerous individual effects and an epistatic interaction network influencing both physiological and expression traits. The interaction effects, which tended to be weak, identified genetic elements that potentially influence the traits and informed on the general genetic architecture of these traits.

The two factors with the largest influence on most phenotypes were sex and diet. Sex influenced all traits except serum leptin levels. In our network, sex also interacted with 14 genetic loci. Although multiple sex-specific QTL have been mapped in humans (Weiss *et al.* 2006; Ober *et al.* 2008), the studies are often of low power and few individual results have been replicated (Ober *et al.* 2008). The DO mice offer a powerful platform to investigate the role of sex in complex traits in mammalian systems. In our study, the majority of the genetic interactions with sex were a suppression of allele effects in males. These alleles may help identify important risk and protective alleles for metabolic disease in females. For example, the 129 allele at a locus on Chr 19 had positive effects on the Metabolism Expression Module and triglyceride levels, suggesting that this locus contains a gene that increases triglycerides through gene expression differences in metabolic pathways. The effects of the 129 allele were suppressed by sex, indicating that it had a larger effect in females than males. Combining the allele and interaction information from the CAPE network, we can generate a hypothesis about the causal gene in this locus. There are six genes known to influence triglycerides in the Chr 19.4 locus and one of these, *Sorbs1*, has a *cis* 129-specific effect increasing *Sorbs1* expression

(Figure 8A). *Sorbs1* is furthermore expressed more highly in females ($p = 0.002$) (Figure 8B), and is significantly correlated with triglyceride levels in the DO mice ($r^2 = 0.17$, $p < 2x10^{-16}$). Previous work has shown that mice with homozygous deletions of this gene have reduced triglyceride levels (Lesniewski *et al.* 2007). Increased expression due to the gain-of-function 129 allele is consistent with increased triglycerides in carriers, and therefore the 129 allele of this gene may increase risk for elevated triglyceride levels in female mice.

In addition to sex, diet is an important factor in determining risk of metabolic disease and their related phenotypes. The high-fat diet in our study had a substantial impact on all traits except the Metabolism Module. High-fat diet enhanced the effects of sex indicating that males in the DO population were more susceptible to the effects of the diet than females. It has been shown that inbred male B6 mice gain more weight and have higher blood lipid profiles when given a high-fat diet (Hwang *et al.* 2010). And although not represented in the DO, male BALB/cA mice have also been shown to be more susceptible than females to weight gain and hepatic lipid accumulation (Nishikawa *et al.* 2007). Diet interacted with a number of genetic loci, and like sex, mostly suppressed the effects of these loci, indicating that the alleles had a larger effect in animals fed standard chow. Multiple studies have shown interactions between genes and diet in influencing factors related to traits associated with metabolic disease (for review see (Ordovas 2006)). The resolution in the DO genome combined with information about genetic interactions will help speed identification of genes interacting with diet and help elucidate how high-fat, high-sucrose diets lead to obesity and metabolic disease, as well as how healthy diets help prevent these conditions.

In addition to the interactions with sex and diet, genetic loci also interacted with each other to influence phenotypes in network motifs. In a previous study of an F_2 intercross (Tyler *et al.* 2016), we found that suppressing-coherent and enhancing-incoherent motifs were significantly enriched in the epistatic network. In this F_2 population, both types of motifs tended to have moderating effects on phenotypes.
The suppressing-coherent network motifs tended to reflect redundancy, while the enhancing-incoherent interactions had a balancing phenotypic effect driving phenotypes toward inbred strain means (Tyler *et al.* 2016). Animals homozygous for one parental allele at both interacting loci had less extreme phenotypes than those with a mix of parental alleles at the two loci (Tyler *et al.* 2016). Similar to our previous findings, network motifs in the DO were predominantly enhancing-incoherent or suppressing-coherent (Figure 6B). However, in contrast to the intercross, the enhancing-incoherent motifs frequently drove traits farther from the population mean than predicted by the additive model. The majority of the suppressing-coherent motifs had redundant effects, *i.e.* the two loci had less than additive effects, but a substantial fraction (36%) also destabilized phenotypes, driving them away from the population mean.

This phenotypic destabilization is likely due to the difference in allelic combinations between the multi-parent DO mice and a classic intercross design. In an intercross all interactions by definition are between alleles from a single non-reference parent, whereas interactions in the DO were most frequently between alleles from different parental ancestries. In both designs, each of the parental strains has developed its own unique set of alleles to maintain quantitative traits at strain homeostasis. In an intercross, accumulation of alleles from a single parental strain may combinatorially achieve homeostatic phenotypes for that parent. By contrast, in the DO the mixing of parental alleles may instead destabilize phenotypes by driving them to extremes and creating the immense phenotypic diversity seen in this population. Furthermore, that we see more destabilizing interactions among the enhancing-incoherent motifs may imply something about molecular pathway structure. We hypothesize that suppressing-coherent motifs represent interactions between genes within a single pathway, while enhancing-incoherent motifs represent interactions between genes in different, but functionally related pathways. This is consistent with earlier work on perturbations of

fruit fly signaling pathways (Horn *et al.* 2011; Carter 2013). The patterns of stabilizing and destabilizing motifs in our study suggests that recombining parental alleles within pathways is well tolerated and often redundant, while recombination between related pathways more frequently destabilizes phenotypes.

Although the genetic diversity in the DO allows relatively fine mapping, we cannot definitively identify which genes in these loci are responsible for the phenotypic effects. We can, however, combine the information in epistatic interactions with estimated functional interactions to generate hypotheses about causal genes. For example, we found an interaction between the A/J haplotype on Chr 9 locus 2 (Chr 9.2: 5 Mb to 36 Mb) and the CAST haplotype on Chr 2 locus 2 (Chr2.2: 123 Mb to 133 Mb) that influenced the Immune Module. Each locus had a negative main effect on the Immune Module, and their combined effect was redundant with the effect of the Chr 2.2 locus (Figure 9A). This pattern of effects indicates a redundant interaction and the possibility that the causal genes on the two loci operate in the same pathway. To further investigate this premise, we identified all the genes in the two regions that had strain-specific polymorphisms (A/J on Chr 9.2 and CAST on Chr 2.2), and filtered these to include genes that had been previously annotated to the mammalian phenotype (MP) term "immune phenotype" (see Methods). We then used Integrative Multi-species Prediction (IMP) (Wong *et al.* 2015) to identify the most likely among these genes to interact functionally. This filtering process identified *Casp4* on Chr 9.2 and *Il1b* on Chr 2.2 as the most likely genes in these two loci to interact. In the IMP network, the two genes interacted directly in a network functionally enriched for cytokine production and secretion ($p = 4.3x10^{-12}$) (Motenko *et al.* 2015) (Figure 9B). In support of the hypothesis that *Casp4* and *Il1b* interact, both transcripts are correlated with the Immune Module (Figure 9C, *Casp4:* $r^2 = 0.48$, $p = 2.6x10^{-28}$, *Il1b:* $r^2 = 0.49$, $p = 1x10^{-30}$), and with each other ($r^2 = 0.32$, $p = 7.4x10^{-13}$) (Figure 8C). *Casp4*, also known as *Casp-11,* is a member of the cysteine-aspartic acid protease family and is essential for IL1B secretion. Mice with homozygous mutations of *Casp4* have decreased levels of circulating IL1B (Wang *et al.* 1998). That *Casp4* is directly involved in IL1B secretion is consistent with the redundant genetic interaction we observed between Chr 9.2 and Chr 2.2 in the CAPE network. Redundant interactions are hypothesized to occur between variants encoding genes within a single pathway (Avery and Wasserman 1992; Lehner 2011). Each variant has a similar effect on the pathway, but because the pathway can only be disrupted once, the combination of the two variants did not have a further effect despite being from different parental strains. Such combinatorial, polygenic candidate genes were revealed by our genetic interaction analysis that identified redundant genetic effects.

Elsewhere in the network, we hypothesize that genes interacting in enhancing-incoherent network motifs function in distinct pathways that nevertheless influence each other. In addition to the redundant interaction above, we prioritized interacting genes in a second interaction between the same A/J haplotype on Chr 9.2 another QTL on Chr 2. This second locus, Chr 2 locus 4 (Chr2.4: 165 Mb to 171 Mb) represented an effect of the NOD haplotype and did not overlap the CAST QTL (123 Mb to 133 Mb) that also interacted with the Chr 9.2 A/J QTL. This QTL thus represents a distinct interaction. The A/J Chr 9.2 and the NOD Chr 2.4 loci influenced the Immune Expression Module in opposite directions, and together, they drove the trait to be slightly more negative than predicted by the additive model (Figure 10A). Following the same gene selection pipeline described above, we identified *Casp4* again for the Chr 9.2 A/J locus, and *Src* as a likely interacting partner in the Chr 2.4 NOD locus (Figure 10B). Transcripts for both genes are significantly correlated with the immune expression module (*Casp4:* $r = 0.47$, $p = 6.3x10^{-28}$; *Src:* $r = 0.47$, $p = 3.7x10^{-27}$) and with each other ($r = 0.21$, $p = 3.2x10^{-6}$) (Figure 10C). In the IMP network *Casp4* and *Src* occupy two lobes of a connected graph, indicating that they are less directly functionally related than *Casp4* and *Il1b*. The *Casp4* side of the network is enriched for genes involved in inflammasome pathways ($p = 2.9x10^{-6}$) (Motenko *et al.* 2015), while the *Src* side of the network is enriched for EGFR signaling ($p = 2.7x10^{-4}$) (Motenko *et al.* 2015). The IL-1 and EGF families of proteins are upregulated in human keratinocytes during wound

healing and in psoriasis, and they have been shown to interact synergistically in upregulating transcripts involved in antimicrobial defenses (Johnston *et al.* 2011). Conversely, inhibiting EGFR signaling in keratinocytes reduces their IL-1 secretion in response to *Staphylococcus aureus* infection (Simanski *et al.* 2016). In sum, these observations suggest that the A/J allele of *Casp4* and the NOD allele of *Src* may interact to influence immune-related expression in mice.

Our analysis of genetic interactions in DO mice has revealed a number of interesting features of the genetic architecture of complex traits related to metabolic disease. First, we detected numerous significant genetic interactions influencing both physiological and expression traits in an outbred population. Although these effects were small relative to the main effects we identified, we were able to detect them by combining information across multiple phenotypes. The interactions primarily involved alleles from different parental haplotypes. This pattern indicates that multi-parent populations may be more powerful platforms than standard intercrosses for detecting epistasis due to the increased genetic diversity. Interactions in an intercross are by definition between alleles from the same parental strain, but in the DO interactions within strain haplotypes are relatively rare. With the additional allelic variation in the DO, more genetic combinations with diverse phenotypic effects are present. Second, we found that network structure of genetic interactions in outbred mice is distinct from the network structure we found previously in a mouse intercross. In the intercross interactions described by network motifs predominantly reduce variation in traits, driving them toward the parental strain mean. In contrast, the enhancing-incoherent motifs in the outbred mice tended to drive traits away from the population mean. The extreme traits were most frequently caused by interactions between allele from different parental haplotypes. Extreme phenotypes upon recombination of alleles in the DO may have the benefit of making epistasis in outbred populations easier to detect than epistasis in intercrosses between two inbred strains. Finally, we showed that we can use genetic interactions as information to prioritize candidate genes in genomic regions. Interactions between two loci imply a functional relationship between elements encoded in the two loci. By combining information about haplotype-specific genetic interactions with genomic functional data, like the IMP network, we can generate plausible hypotheses regarding causal genes. The hypotheses generated by this method in this study were supported by expression data not used in the hypothesis generation. Together these results speak to the value of multi-parent outbred populations in the dissection of the genetic architecture of clinically relevant complex traits.

Methods

Mice

Mice were obtained from The Jackson Laboratory (Bar Harbor, ME) as described in (Svenson *et al.* 2012) and @Gatti. The animals were non-sibling DO mice ranging from generation 4 to 11, and males and females were represented equally. All animal procedures were approved by the Animal Care and Use Committee at The Jackson Laboratory (Animal Use Summary # 06006). Mice were house in same-sex cages with five animals per cage as described in (Svenson *et al.* 2012) and @Gatti. Animals had free access to either standard rodent chow (6% fat by weight, LabDiet 5K52, LabDiet, Scott Distributing, Hudson, NH) or a high-fat, high-sucrose diet (HFD) (Envigo Teklad TD.08811, Envigo, Madison, WI) for the duration of the study protocol (26 weeks). Caloric content of the HFD was 45% fat, 40% carbohydrates and 15% protein. Diets were assigned randomly.

Phenotype Measurements

Phenotypes were measured as described in (Svenson *et al.* 2012) and @Gatti. Beginning at eight weeks of age, blood was collected retro-orbitally after administration of local anesthetic. Cholesterol and triglycerides were measured using the Beckman Synchron DXC600Pro Clinical chemistry analyzer. Leptin was measured in non-fasted plasma prepared as previously described (Svenson *et al.* 2012). Levels were analyzed using the Meso Scale Discovery electrochemiluminescent system

according to the manufacturer's recommended protocol (Meso Scale Diagnostics, Rockville, MD). Body composition (lean mass and total mass) were measured at age 12 weeks using dual X-ray absorptiometry (DEXA) using a Lunar PIXImus densitometer (GE Medical Systems). Fat mass was calculated as log(total mass - lean mass). Measurements were performed at two time points. All measurements in this study were taken from the first time point.

Genetic analysis

Genotyping was performed on tail biopsies as described in (Svenson *et al.* 2012) using the Mouse Universal Genotyping Array (MUGA). A subset of the animals (293) were genotyped on the Megamuga (GeneSeek, Lincoln, NE). The intensities from the arrays were used to infer the haplotype blocks in each DO genome using a hidden Markov model (HMM) (Gatti *et al.* 2014b).

Merging Haplotype Reconstructions from Different Methods

Genotypes were measured with the MUGA (7,854 markers), Megamuga (77,642 markers) and by GBRS, which is a set of software tools that uses RNA-Seq data to reconstruct individual sample genomes in multiparental population (MPP) (@Gatti, and http://https://github.com/churchill-lab/gbrs). To merge diplotype probabilities from all sources, we interpolated markers on an evenly spaced 64,000 marker grid (0.0238 cM between markers).

Transcriptome profiling

Transcriptome-wide expression levels were measured as described in (Chick *et al.* 2016), (Munger *et al.* 2014) and @Gatti. Total liver RNA was isolated from each mouse and sequenced using single-end RNA-Seq (Munger *et al.* 2014). Transcripts were aligned to strain-specific genomes from the DO founders (Chick *et al.* 2016). We used an expectation maximization algorithm (EMASE, https://github.com/ churchill-lab/emase) to estimate read counts. Read counts in each sample were normalized using upper-quantile normalization and a rank Z transformation was applied across samples.

Filtering transcripts for *trans* effects

We were interested in mapping effects to transcripts that were influenced by distant (*trans*) genetic loci. To determine which transcripts had *trans* loci, we first used DOQTL (Gatti *et al.* 2014a) to map QTL for all transcripts expressed in at least 50 samples (26,875 transcripts). DOQTL effects using founder allele haplotype probabilities calculated as described in (Gatti *et al.* 2014b). In addition, we used sex, diet and batch as additive covariates and used hierarchical linear models to correct for genetic relatedness (Kang *et al.* 2008).

From this mapping we identified *cis*-eQTLs for transcripts, which we defined as a suggestive eQTL (LOD >=7.4) within 2 Mbp of the encoding gene's transcription start site. For each transcript, we regressed out the effects of the *cis*-eQTL (Pierce *et al.* 2014) and re-mapped QTL using DOQTL. We identified 3635 trans-eQTLs defined as a QTL (LOD >= 7.4) on a chromosome other than the transcripts encoding gene or at least 10 Mb away on the same chromosome. Additionally, for the following clustering analysis, we used the residual expression by removing the effects of *cis-haplotype* and batch effect via linear regression. The procedure is outlined in Supplementary Figure 1.

Weighted Gene Co-expression Network Analysis

Co-expression gene modules were obtained by clustering *trans*-acting transcripts using the WGCNA package in R (Langfelder and Horvath 2008; undefined author 2016). WGCNA computes the absolute value of Pearson correlation for all gene pairs and generates an adjacency matrix by raising the

correlation matrix to a user-defined power. We set the power to six to achieve a network with scale-free degree distribution. To construct the module network, WGCNA uses hierarchical clustering to produce a dendrogram of genes. Individual branches of the dendrogram represent modules, which are clusters of highly co-expressed genes. The modules with similar expression profiles can be merged based on their correlation. We set the minimum module size to 30 and the minimum height for merging to 0.25 (corresponding to a Pearson correlation of 0.75) to obtain relatively large and distinct modules. The first principal component for each module (termed *eigengenes* in WGCNA) is used to represent the summary co-expression pattern for each module. These eigengenes are hereafter referred to as *module phenotypes* for CAPE analysis. Each module was assessed for functional enrichment using the DAVID database(Huang *et al.* 2009a; b). The GO enrichment significance threshold for all gene ontology enrichment analyses was $p \leq 0.05$, with Benjamini correction for multiple comparisons.

Combined analysis of pleiotropy and epistasis

Combined analysis of pleiotropy and epistasis (CAPE) is a method for deriving genetic interaction networks of genetic variants that influence multiple phenotypes {tyler2013cape}. The open-source R package of cape was adapted (below) to use for DO mice with extension to multiple alleles in our analysis.

We began our analysis by regressing outbreeding generation out of each trait and applying a rank Z transformation to each physiological trait. These were combined with the three module eigengenes representing significantly enriched modules from WGCNA (see above). We then performed singular value decomposition (SVD) on the trait matrix to obtain eight orthogonal eigentraits (ET's). The ET's combine common signals across all traits. In this analysis, we used the first three ETs, which captured 88.3% of the variation in the traits. We then performed linear regression to associate each marker with each ET.

For each marker we used a seven-state model to estimate the effect of the founder haplotypes on each trait. We use the B6 allele as the reference, and thus B6 alleles are not explicitly included in our final results. We also included two covariates, sex (female: 0, male: 1) and diet (chow: 0, high-fat: 1).

$$E_i^j = \beta_0^j + \underbrace{\sum_{c=1}^{2} x_{c,i}\beta_c^j}_{\text{covariates}} + \underbrace{\sum_{a=1}^{7} P_{i,a}\beta_a^j}_{\text{allele effects}} + \epsilon_i^j$$

The index i is from 1 to number of samples and j is from 1 to number of ET's.
$P_{i,a}$ is the probability of each allele a at the locus, and $x_{c,i}$ is the presence or absence of each covariate.
We used the results of the single-locus regression to select markers for the locus-pair regressions.

Variant selection for pairwise regression

Because there were more markers genotyped than could be tested in a pairwise regression, we selected a subset of variants based on standardized effect size. We selected individual haplotypes (for example the A/J haplotype at marker 1) such that haplotypes from multiple founder strains and multiple chromosomes would be represented in the locus-pair regression. To do this, we picked an arbitrary threshold and identified haplotype peaks in effect size that rose above this threshold. We picked the marker with the largest effect size in this peak and sampled 10% of the remaining markers in the peak uniformly at random. We progressively lowered the threshold until we had sampled approximately 500 individual variants. (Supplementary Table 2) The final number of variants selected was 515, representing all haplotypes across 17 chromosomes.

Pairwise regression

We express the full model for two variants labeled 1 and 2 as:

$$E_i^j = \beta_0^j + \underbrace{\sum_{c=1}^{2} x_{c,i}\beta_c^j}_{\text{covariates}} + \underbrace{P_{1,i}\beta_1^j + P_{2,i}\beta_2^j}_{\text{main effects}} + \underbrace{P_{1,i}P_{2,i}\beta_{12}^j}_{\text{interaction}} + \epsilon_i^j$$

The index i is from 1 to number of samples and j is from 1 to number of ET's.
$P_{i,a}$ is the probability of each allele a at the locus, and $x_{c,i}$ is the presence or absence of each covariate.
Eij is the ET for sample i. $P_{1,i}$ and $P_{2,i}$ are the probabilities of the allele at each of two variants for sample i. $P_{1,i}$ $P_{2,i}$ is the interaction of two variants, β_1 and β_2 are the effects of two variants on the ET j, and β_{12} is the interaction coefficient.

For each marker pair, the regression coefficients across all ET's were reparametrized to obtain two new parameters (δ_1 and δ_2). The δ terms are independent of phenotype and can be defined as the degree to which one variant influences the effect of the other on the phenotypes. δ_1 represents the inferred genetic activity of the first variant when the second variant is present. A negative δ coefficient indicates one variant suppressing another. For example, a negative δ_1 indicates that variant 1 suppresses the effect of variant 2 on that phenotype. The δ terms are computed in terms of coefficients from pairwise regression as follows:

$$\begin{bmatrix}\delta_1\\ \delta_2\end{bmatrix} = \begin{bmatrix}\beta_1^1 & \beta_2^1\\ \beta_1^2 & \beta_2^2\\ \vdots & \vdots\end{bmatrix}^{-1} \cdot \begin{bmatrix}\beta_{12}^1\\ \beta_{12}^2\\ \vdots\end{bmatrix}$$

Next, the δ terms are translated into directed variables m_{12} and m_{21}, which describe variant-to-variant influences that fit all phenotypes via indirect associations. The term m_{12} and m_{21} are direct influences of one variant on the other, with negative influences indicating suppression and positive influences indicating enhancement. The terms m_{12} and m_{21} are defined in terms of δ_1 and δ_2:
$m_{12} = \frac{\delta_1}{1+\delta_2}, m_{21} = \frac{\delta_2}{1+\delta_1}$
Errors are estimated through standard least-squares regression and a second-order Taylor expansion on the regression parameters (Carter *et al.* 2012). We defined the absolute value of the ratio of an estimated coefficient and its standard error ($|\beta/se|$) as the standardized effect to evaluate the main effects of the variants on the phenotypes and the interactive effects of the variants. The significance threshold of the standardized effect is determined based on genotype permutation test and adjusted for multiple testing. To avoid false positives due to linkage disequilibrium (LD), we excluded variant pairs with Pearson's correlation coefficient above 0.5 in the pairwise regression.

Permutation testing

Permutation testing was conducted to generate null distributions of m parameters. For each permutation, we shuffled the ETs relative to genotypes. We then performed a single locus scan and selected the top ~500 markers for a pairwise marker scan as described above. We repeated this process until 500,000 marker pairs were tested. We combined permutations across marker pairs to generate a single null distribution (Tyler *et al.* 2014). Empirical p values for each model parameter were calculated and corrected using false discovery rate (FDR) {benjamini1995controlling}.

Grouping linked markers

Final results are reported for linkage blocks rather than individual markers. The blocks were determined as described in (Tyler *et al.* 2016). Briefly, for each haplotype, we used the correlation matrix between variants as an adjacency matrix to construct a weighted network, and used the fast greedy community detection algorithm in R/igraph to estimate boundaries between blocks of similar markers (Csardi and Nepusz 2006).

Phenotypic Effects of Motifs

For each motif in the epistatic network, we examined the phenotypic effects of each of the individual loci as well as the interaction effect. For each individual locus, we divided the animals into two bins: those carrying the alternate allele (e.g. at least heterozygous for the A/J allele at locus 1), and all others. We calculated the mean trait value across all traits for both groups, and defined the main effect of the allele as the difference between the groups. The predicted additive effect was the sum of the two main effects. To calculate the actual effect of the interaction, we binned the animals into two groups: those carrying the alternate allele at both loci (e.g. at least heterozygous for the A/J allele at locus 1 *and* at least heterozygous for the NOD allele at locus 2), and all others.

Prioritization of genes in interacting loci

We used a function-oriented method to generate hypotheses about which genes in interacting regions might be contributing to the epistatic effects inferred by CAPE. We focused on two interactions that influenced the Immune Module, the module eigengene from the gene module enriched for immune function. Both interactions involved the A/J haplotype from a region on Chr 9. This region interacted with the NOD haplotype on Chr 2 and the CAST haplotype on Chr 2 to influence the Immune Module. We first used biomaRt found all protein coding genes in the region by finding all genes in the effect size peak created by the haplotype (Durinck *et al.* 2005; 2009). We used the R package SNPTools (Gatti) to query the Sanger SNP database (Keane *et al.* 2011; Yalcin *et al.* 2011) to find genes harboring variants private to the strain of interest. Thus, we found all private A/J variants in the region defined by the A/J effect on Chr 9, and all variants private to NOD and CAST on the Chr 2 regions defined by these haplotype effects respectively.

Because the main effects of these regions were related to the immune module, we further filtered the genes in each region to genes annotated to the Mouse Phenotype (MP) Ontology(Smith *et al.* 2005) term “immune phenotype.” We then looked for the most probable functional interactions between the groups of genes from each chromosomal region using Integrative Multi-species Prediction (IMP) (Wong *et al.* 2015). IMP is a Bayesian network built through integration of gene expression data, protein-protein interaction data, gene ontology annotations and other data. It predicts the likelihood that pairs of genes interact functionally in multiple model organisms and humans. We used IMP to find the highest likelihood connected component that contained at least one gene from each chromosomal region participating in the epistatic interaction. We selected the gene pair with the highest likelihood of interacting functionally as our top candidate gene pair for the interaction.

Figures

Module	# Genes	Enriched GO Terms (Benjamini adjusted p value)
Metabolism Module	1192	Cellular macromolecular metabolic process ($6.3x10^{-17}$) Biosynthetic process ($1.6x10^{-5}$)
Redox Module	208	Oxidation-reduction process ($7.7x10^{-7}$) Fatty acid metabolic process ($5.7x10^{-2}$)
Immune Module	186	Immune system process ($5.2x10^{-2}$) Cell adhesion ($7.9x10^{-15}$)

Table 1. Functional enrichment for three gene expression modules found by WGCNA.

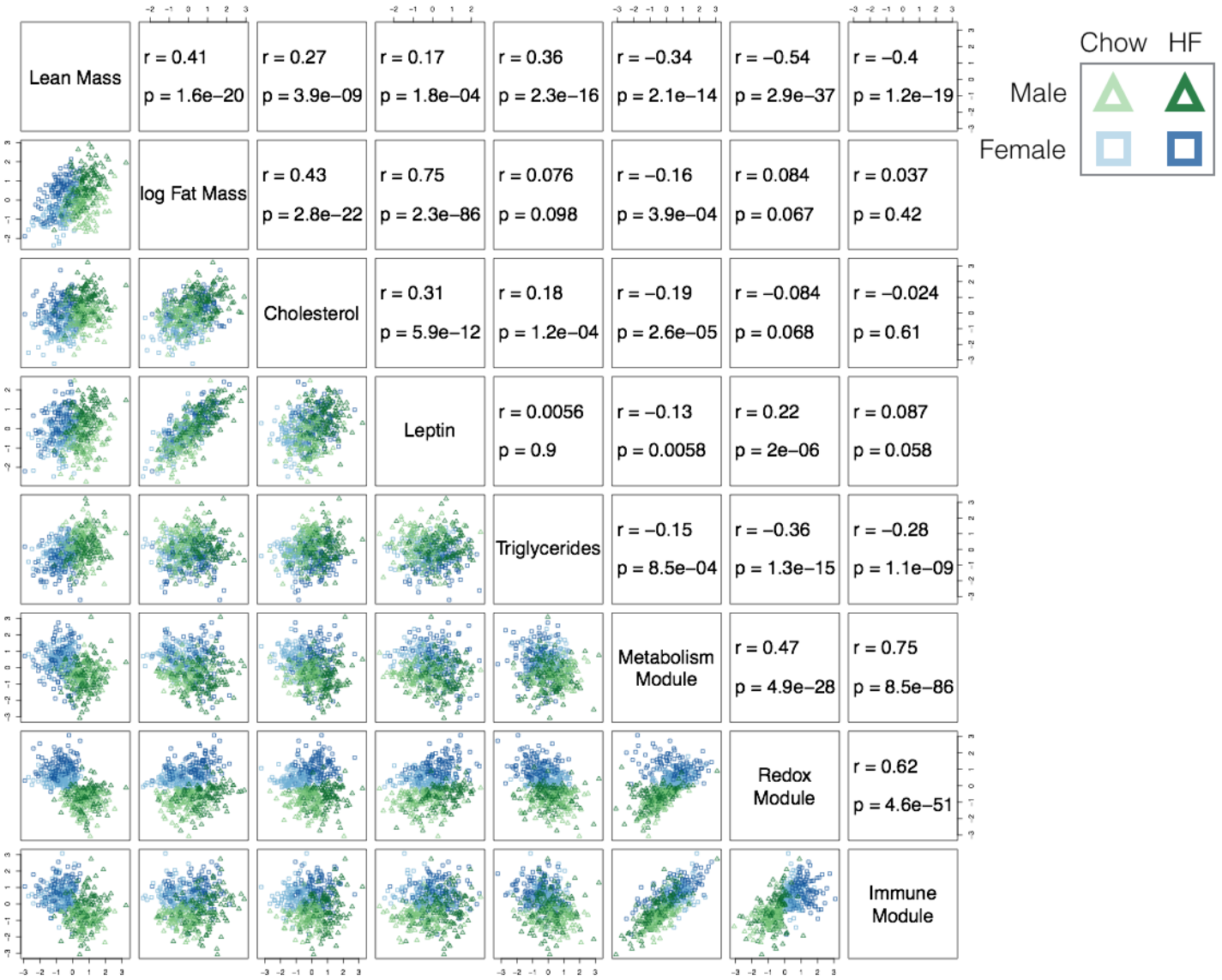

Figure 1. Correlation plots for all phenotypes used in this study. Traits tend to be modestly correlated with each other. Physiological traits and expression traits are positively correlated within their groups, but negatively correlated between groups. Males are shown as green triangles and females are blue squares. Darker shade indicates high-fat diet (HF).

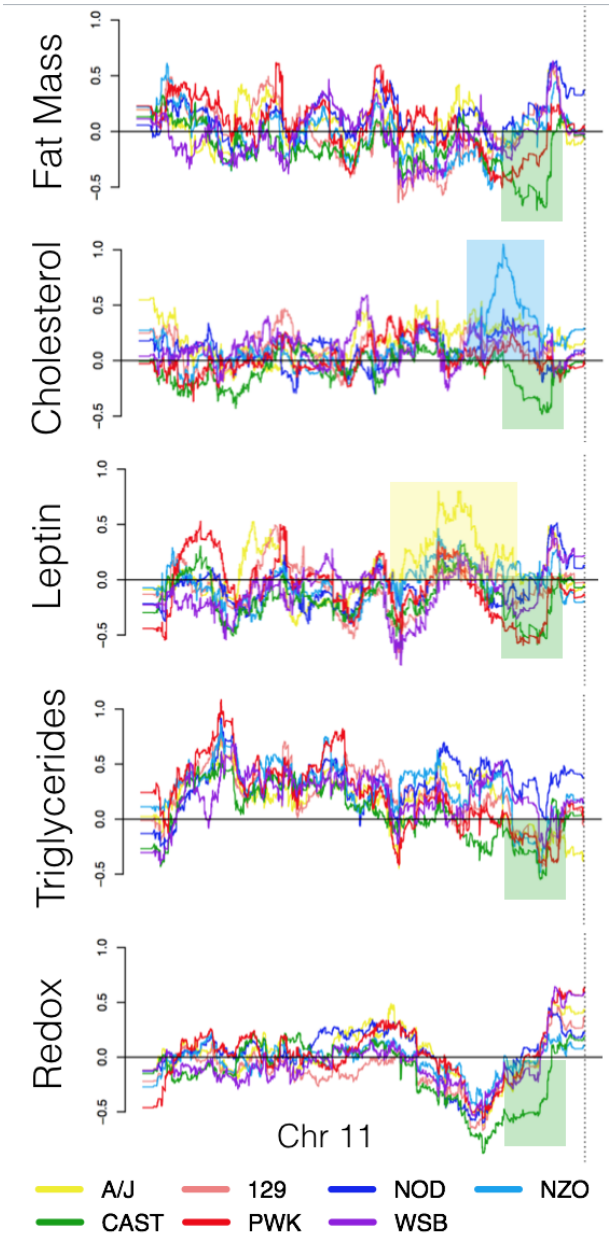

Figure 2. Effect sizes of each strain haplotype on Chr 11 on five traits: lean mass, log fat mass, cholesterol, triglycerides, and the metabolism expression module. Individual haplotypes have distinct effects on traits. The CAST haplotype on distal Chr 11 has pleiotropic effects on all traits (green boxes). The NZO and A/J haplotypes have individual effects on cholesterol (blue box)and leptin (yellow box) respectively.

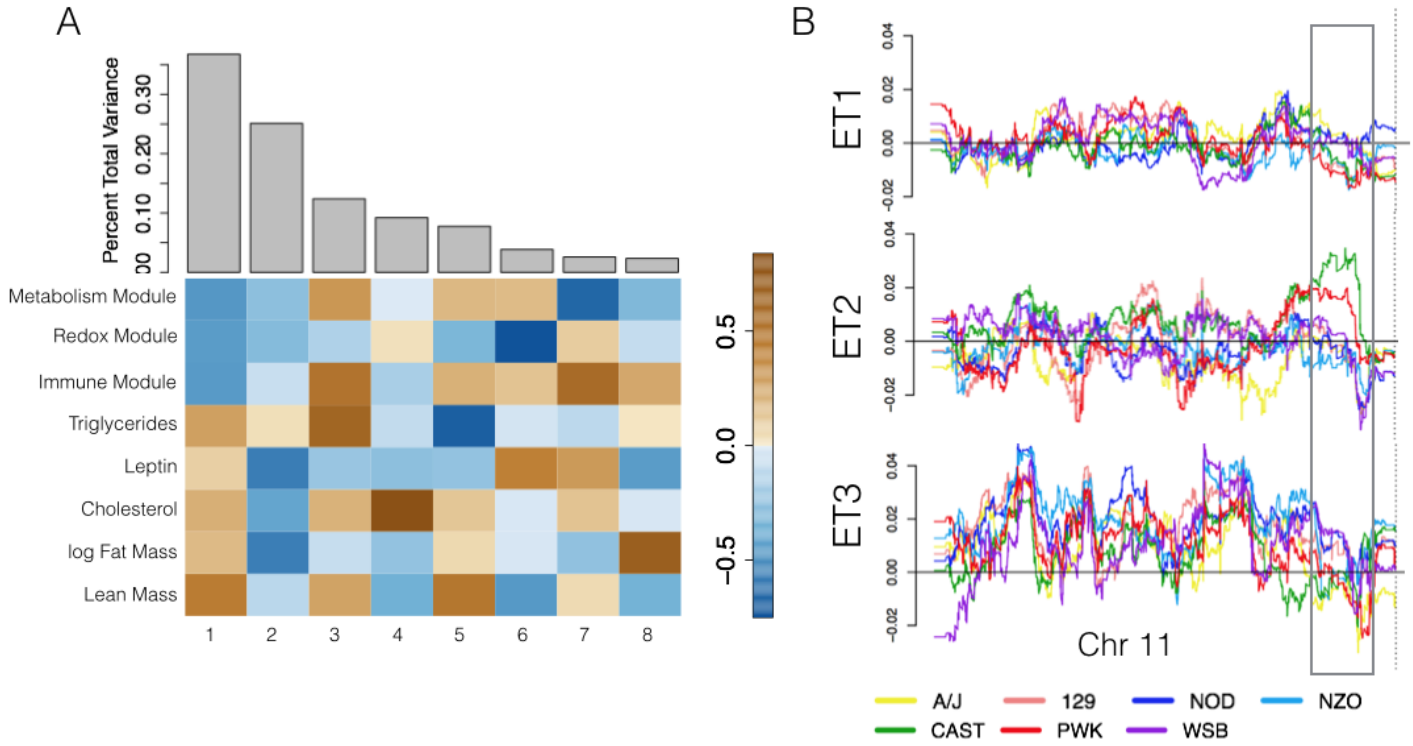

Figure 3. Eigentrait (ET) selection from decomposition of traits. A) Traits were decomposed by singular value decomposition (SVD) to orthogonal ETs. The gray bars show the proportion of the total variance captured by each ET, and the heatmap shows relative contributions of each trait to each ET. B) Haplotype effects for Chr 11 on the first three ETs.

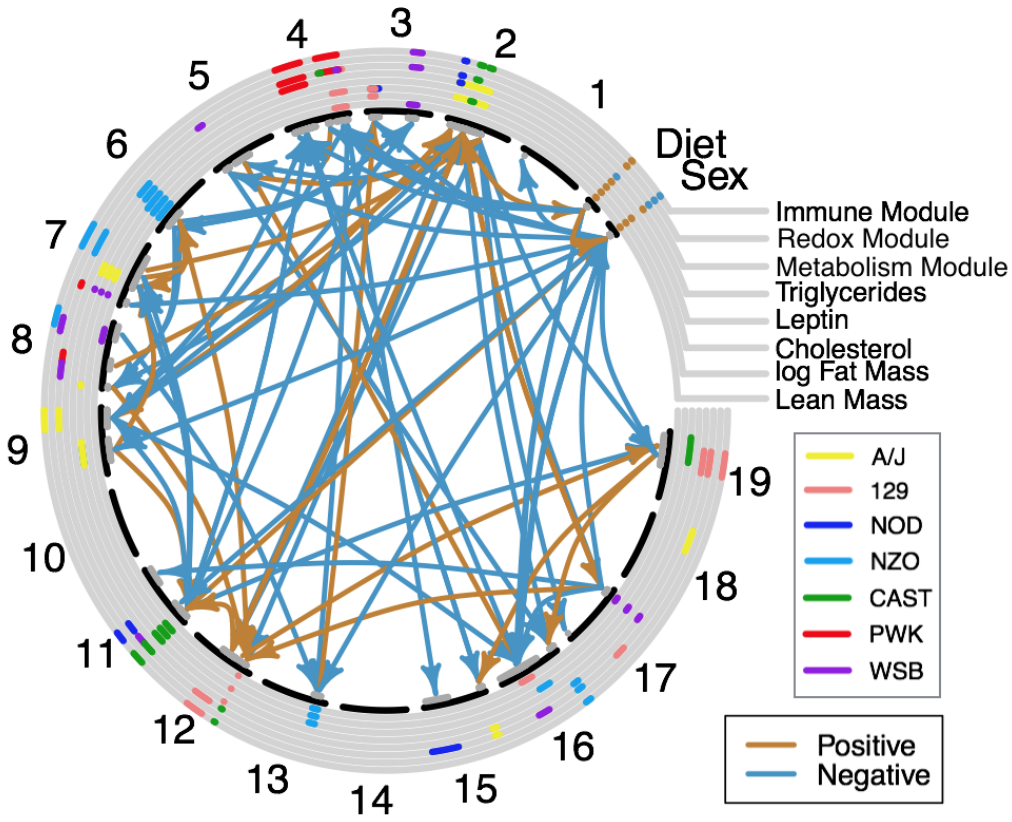

Figure 4. The final locus interaction network. Main effects are shown in gray concentric circles. Significant main effects are colored for the haplotype that had the significant effects. Positive (brown) and negative (blue) effects are only shown for Sex and Diet. Interactions are shown as arrows between chromosomal regions and are colored to indicate an enhancing effect (brown) or a suppressing effect (blue).

A

	Source	Target	Total	Rep	#Chrs
WSB	18	14	32	70	12
CAST	12	16	28	82	7
A/J	12	15	27	100	8
129	5	21	26	87	8
Sex	12	3	15	-	-
NOD	6	6	12	32	6
PWK	4	6	10	60	4
NZO	14	7	8	84	9
Diet	6	1	7	-	-

B

	CAST	PWK	129	WSB	NZO	A/J	NOD	Diet	Sex
CAST	1	2	2	1	-	3	1	1	1
PWK	2	-	1	-	-	1	-	-	-
129	2	-	-	-	1	2	-	-	-
WSB	2	1	4	5	4	-	1	-	1
NZO	2	-	5	3	-	3	1	-	-
A/J	2	2	2	2	1	1	2	-	-
NOD	2	-	1	-	-	3	-	-	-
Diet	2	-	2	-	-	1	-	-	1
Sex	1	1	4	3	1	1	1	-	-

Figure 5. Tabulation of allele participation in epistatic interactions. A) The number of times each haplotype was the source of an interaction or the target of an interaction, and the total number of interactions each haplotype participated in. Rows are sorted by total number of interactions. The final two columns indicate how many markers were tested in the pairwise marker tests for each haplotype, and how many chromosomes these markers were found on. Darker blue highlighting indicates higher counts. B) A detailed count of the interactions each haplotype participated in with each other haplotype and each covariate (Sex and Diet). Darker blue squares represent higher counts. Counts of 0 are represented by dashes for visualization purposes.

A

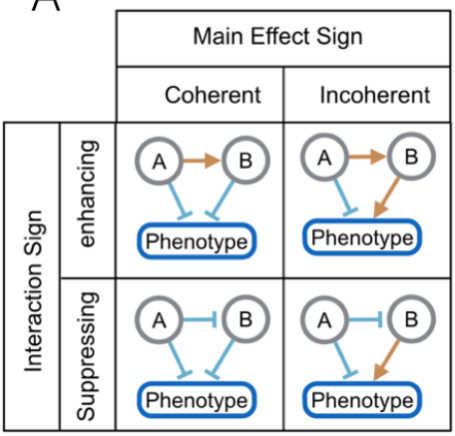

B

	enhancing		suppressing	
	incoherent	coherent	incoherent	coherent
Lean Mass	2	0	0	4
Fat Mass	2	0	0	4
Chol	9	0	0	8
Leptin	1	0	0	2
TG	6	0	0	5
Metabolism	13	0	0	16
Redox	0	0	0	0
Immune	8	0	0	8

Figure 6. Network Motifs A) Cartoons depicting four types of network motif. Each motif consists of two markers interacting to influence one phenotype. The markers can either have the same (coherent) or different (incoherent) main effect. The interaction between them can be either enhancing or suppressing. B) Counts of each different motif type for each phenotype. Darker shades of blue indicate higher counts.

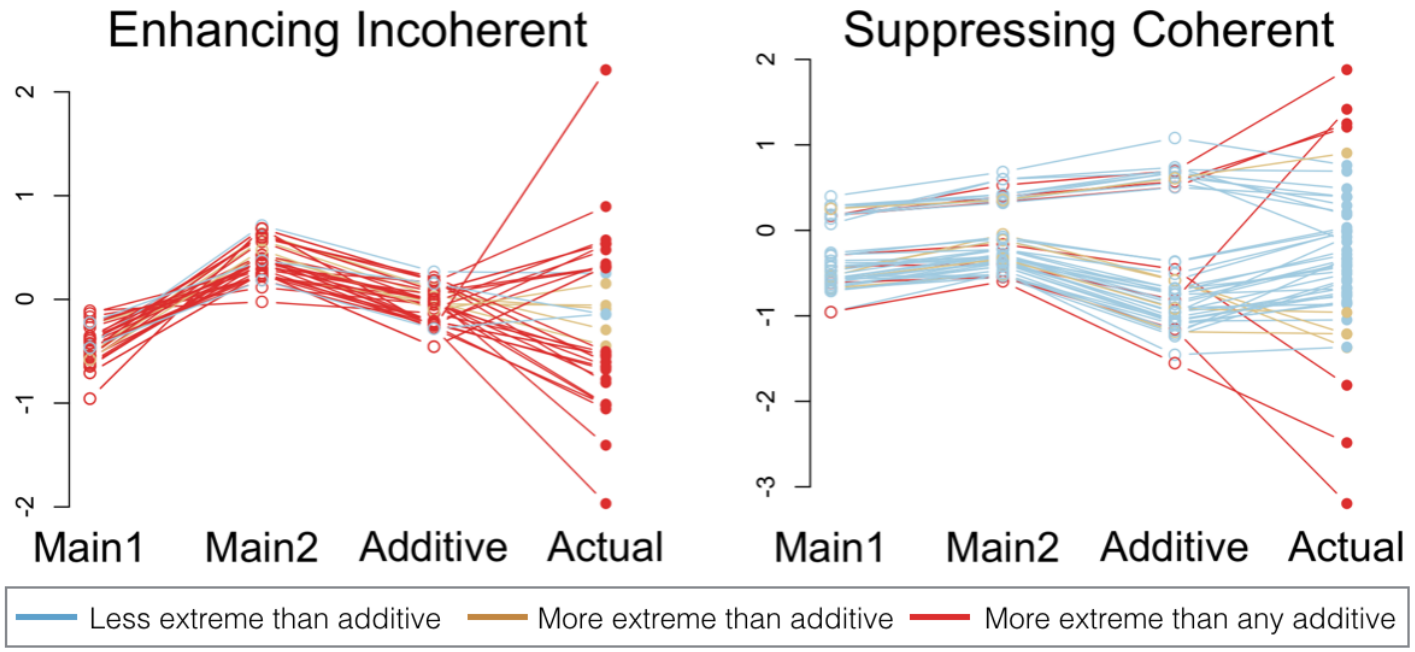

Figure 7. Phenotypic effects of enhancing-incoherent (left) and suppressing-coherent (right) network motifs. "Main1" and "Main2" show the average deviation from population mean in normalized phenotype for animals carrying the alternate allele at marker 1 and marker 2 in the motif respectively. Marker 1 and marker 2 are sorted such that marker 1 always has the smaller (more negative) effect. "Additive" shows the predicted additive effect given the Main1 and Main2 effects. "Actual" shows the actual deviation from the population mean of animals carrying the alternate allele at both marker 1 and marker 2 in the motifs. Lines are drawn to connect dots from individual motifs. Blue lines indicate motifs that bring phenotypes closer to the population mean than predicted by the additive model. Brown lines indicate motifs that drive the phenotype farther from the population mean than predicted by the additive model. Red lines indicate a subset of motifs that create more extreme phenotypes than predicted by any additive model.

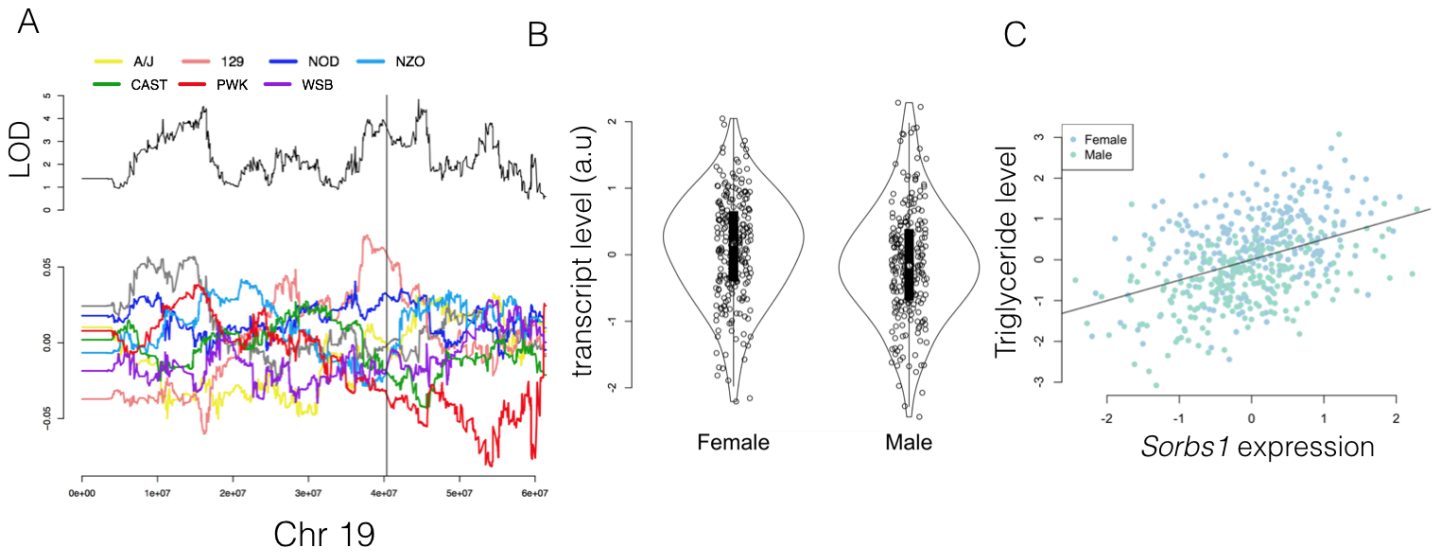

Figure 8. Evidence supporting a role of the 129 allele of *Sorbs1* increasing triglyceride levels through increased transcription. A) LOD score (top) and haplotype coefficients (bottom) for expression of *Sorbs1.* The vertical black line marks the position of *Sorbs1* in the genome on Chr 19. B) Expression of Sorbs1 in male and female DO mice (a.u. = arbitrary units).. C) Correlation between triglyceride levels and *Sorbs1* expression ($r = 1.7$, $p < 2x10^{-16}$). Female mice are shown in blue, and males are shown in green.

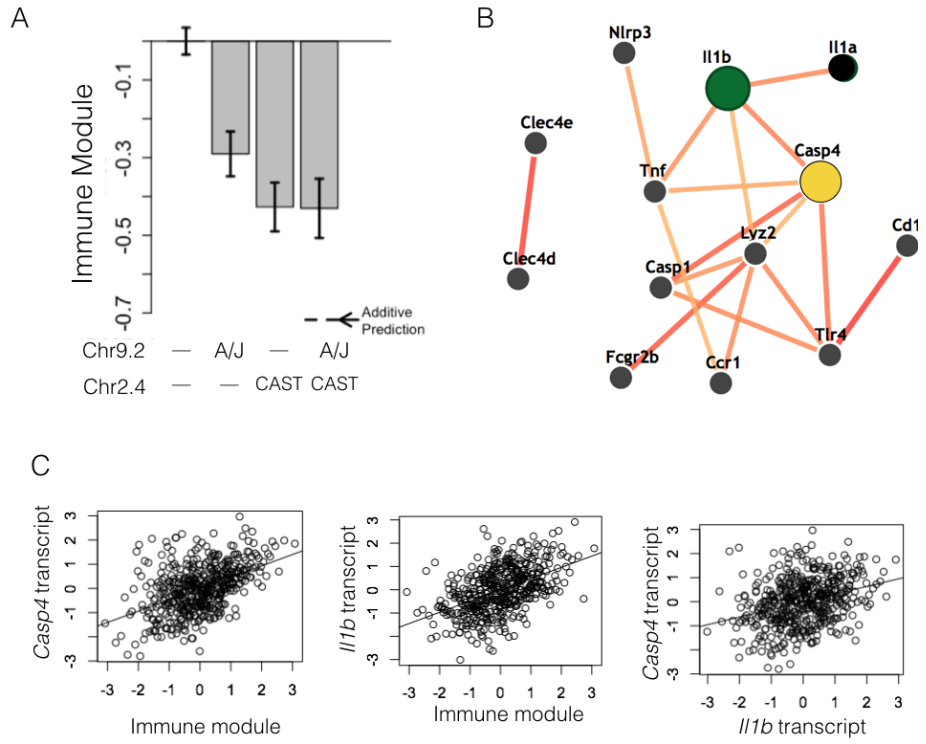

Figure 9. Gene prioritization in interacting loci. A) Effects of an interaction between Chr 9 locus 2 (Chr 9.2) and Chr 2 locus 2 (Chr 2.2). The A/J haplotype on Chr 9.2 and the CAST haplotype on Chr 2.2 have individual negative effects on the Immune Module. Together, they have the same effect as the CAST allele on Chr 2.2, indicating a redundant interaction. Error bars show standard error. B) The transcripts of Casp4, on Chr 9, and Il1b, on Chr 2, are both correlated with the Immune Module. The transcripts are also correlated with each other. C) The functional connections between *Casp4* and *Il1b* from the IMP network. The two genes are predicted to interact functionally with high confidence.

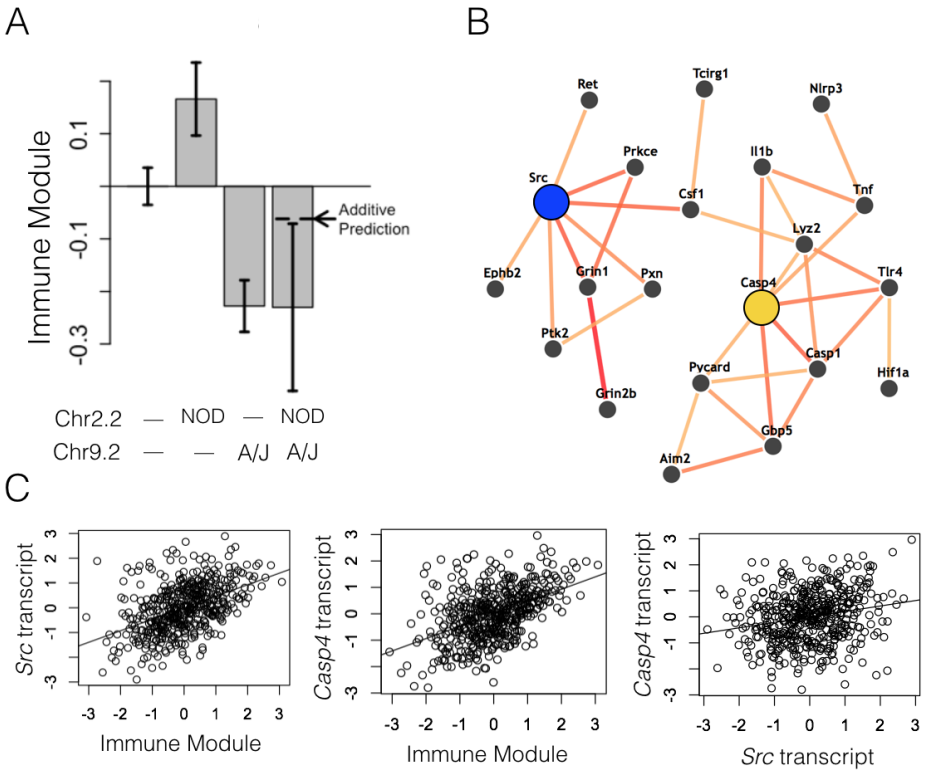

Figure 10. Gene prioritization in interacting loci. A) Effects of an interaction between Chr 9 locus 2 (Chr 9.2) and Chr 2 locus 2 (Chr 2.4). The A/J haplotype on Chr 9.2 has a negative effect on the Immune Module and the NOD haplotype on Chr 2.4 has a positive effect on the Immune Module. Together, they have an effect similar to that of the A/J allele on Chr 9.2. Error bars show standard error. B) The transcripts of Casp4, on Chr 9, and Src, on Chr 2, are both correlated with the Immune Module. The transcripts are also correlated with each other. C) Functional connections between *Src* and *Casp4* from the IMP network. The two genes are predicted to interact functionally by operating in related, but distinct pathways.

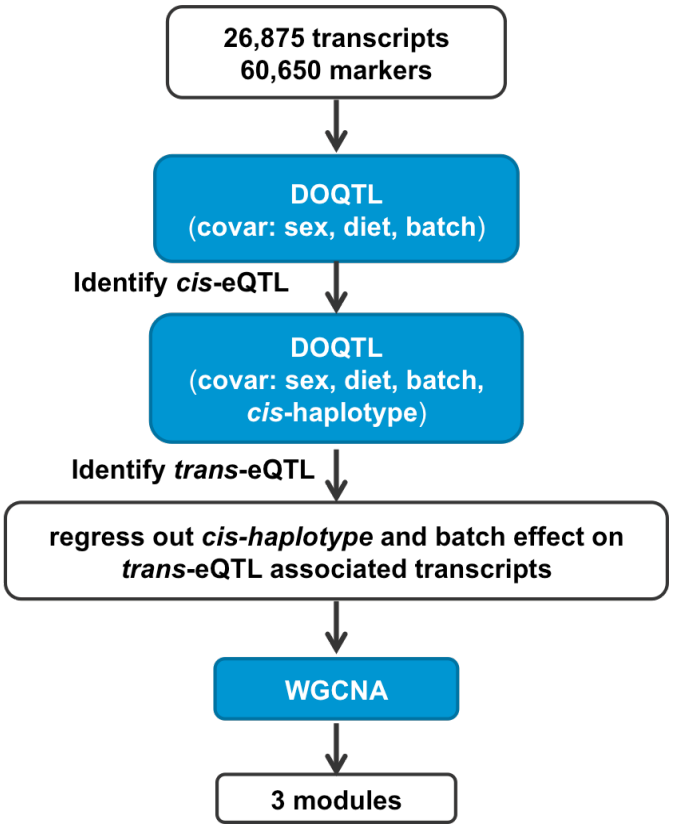

Supplementary Figure 1. Analysis pipeline to generate co-expression modules

Avery L., Wasserman S., 1992 Ordering gene function: the interpretation of epistasis in regulatory hierarchies. Trends Genet. **8**: 312–316.

Bogue M. A., Churchill G. A., Chesler E. J., 2015 Collaborative Cross and Diversity Outbred data resources in the Mouse Phenome Database. Mamm Genome **26**: 511–520.

Carter G. W., 2013 Inferring gene function and network organization in Drosophila signaling by combined analysis of pleiotropy and epistasis. G3 (Bethesda) **3**: 807–814.

Carter G. W., Hays M., Sherman A., Galitski T., 2012 Use of pleiotropy to model genetic interactions in a population. PLoS Genet. **8**: e1003010.

Chesler E. J., Gatti D. M., Morgan A. P., Strobel M., Trepanier L., Oberbeck D., McWeeney S., Hitzemann R., Ferris M., McMullan R., Clayshultle A., Bell T. A., de Villena F. P.-M., Churchill G. A., 2016 Diversity Outbred Mice at 21: Maintaining Allelic Variation in the Face of Selection. G3 (Bethesda) **6**: 3893–3902.

Chick J. M., Munger S. C., Simecek P., Huttlin E. L., Choi K., Gatti D. M., Raghupathy N., Svenson K. L., Churchill G. A., Gygi S. P., 2016 Defining the consequences of genetic variation on a proteome-wide scale. Nature **534**: 500–505.

Csardi G., Nepusz T., 2006 The igraph software package for complex network research. InterJournal **Complex Systems**: 1695.

Durinck S., Moreau Y., Kasprzyk A., Davis S., De Moor B., Brazma A., Huber W., 2005 BioMart and Bioconductor: a powerful link between biological databases and microarray data analysis.

698 Bioinformatics **21**: 3439–3440.

699 Durinck S., Spellman P. T., Birney E., Huber W., 2009 Mapping identifiers for the integration of
700 genomic datasets with the R/Bioconductor package biomaRt. Nat Protoc **4**: 1184–1191.

701 Forbes G. B., 1987 Lean Body Mass-Body Fat Interrelationships in Humans. Nutrition Reviews **45**:
702 225–231.

703 Gatti D. M., SNPtools. 2013, https://CRAN.R-project.org/package=SNPtools.

704 Gatti, Daniel M., et al. "Quantitative trait locus mapping methods for diversity outbred mice." *G3:*
705 *Genes| Genomes| Genetics* 4.9 (2014): 1623-1633.

706 Gatti D. M., Svenson K. L., Shabalin A., Wu L.-Y., Valdar W., Simecek P., Goodwin N., Cheng R., Pomp D.,
707 Palmer A., Chesler E. J., Broman K. W., Churchill G. A., 2014b Quantitative trait locus mapping
708 methods for diversity outbred mice. G3 (Bethesda) **4**: 1623–1633.

709 Ghazalpour A., Doss S., Bin Zhang, Wang S., Plaisier C., Castellanos R., Brozell A., Schadt E. E., Drake T.
710 A., Lusis A. J., Horvath S., 2006 Integrating Genetic and Network Analysis to Characterize Genes
711 Related to Mouse Weight. PLoS Genet. **2**: e130.

712 Greene C. S., Penrod N. M., Williams S. M., Moore J. H., 2009 Failure to replicate a genetic association
713 may provide important clues about genetic architecture. (TIA Sorensen, Ed.). PLoS ONE **4**: e5639.

714 Horn T., Sandmann T., Fischer B., Axelsson E., Huber W., Boutros M., 2011 Mapping of signaling
715 networks through synthetic genetic interaction analysis by RNAi. Nat. Methods **8**: 341–346.

716 Huang D. W., Sherman B. T., Lempicki R. A., 2009a Systematic and integrative analysis of large gene
717 lists using DAVID bioinformatics resources. Nat Protoc **4**: 44–57.

718 Huang D. W., Sherman B. T., Lempicki R. A., 2009b Bioinformatics enrichment tools: paths toward the
719 comprehensive functional analysis of large gene lists. Nucleic Acids Res. **37**: 1–13.

720 Huang W., Mackay T. F. C., 2016 The Genetic Architecture of Quantitative Traits Cannot Be Inferred
721 from Variance Component Analysis. (X Zhu, Ed.). PLoS Genet. **12**: e1006421.

722 Hwang L.-L., Wang C.-H., Li T.-L., Chang S.-D., Lin L.-C., Chen C.-P., Chen C.-T., Liang K.-C., Ho I.-K., Yang
723 W.-S., Chiou L.-C., 2010 Sex differences in high-fat diet-induced obesity, metabolic alterations and
724 learning, and synaptic plasticity deficits in mice. Obesity (Silver Spring) **18**: 463–469.

725 Johnston A., Gudjonsson J. E., Aphale A., Guzman A. M., Stoll S. W., Elder J. T., 2011 EGFR and IL-1
726 Signaling Synergistically Promote Keratinocyte Antimicrobial Defenses in a Differentiation-
727 Dependent Manner. Journal of Investigative Dermatology **131**: 329–337.

728 Kang H. M., Zaitlen N. A., Wade C. M., Kirby A., Heckerman D., Daly M. J., Eskin E., 2008 Efficient
729 control of population structure in model organism association mapping. Genetics **178**: 1709–
730 1723.

731 Keane T. M., Goodstadt L., Danecek P., White M. A., Wong K., Yalcin B., Heger A., Agam A., Slater G.,
732 Goodson M., Furlotte N. A., Eskin E., Nellåker C., Whitley H., Cleak J., Janowitz D., Hernandez-
733 Pliego P., Edwards A., Belgard T. G., Oliver P. L., McIntyre R. E., Bhomra A., Nicod J., Gan X., Yuan
734 W., van der Weyden L., Steward C. A., Bala S., Stalker J., Mott R., Durbin R., Jackson I. J., Czechanski
735 A., Guerra-Assunção J. A., Donahue L. R., Reinholdt L. G., Payseur B. A., Ponting C. P., Birney E.,

736 Flint J., Adams D. J., 2011 Mouse genomic variation and its effect on phenotypes and gene
737 regulation. Nature **477**: 289–294.

738 Langfelder P., Horvath S., 2008 WGCNA: an R package for weighted correlation network analysis.
739 BMC Bioinformatics **9**: 559.

740 Lehner B., 2011 Molecular mechanisms of epistasis within and between genes. Trends Genet. **27**:
741 323–331.

742 Lesniewski L. A., Hosch S. E., Neels J. G., de Luca C., Pashmforoush M., Lumeng C. N., Chiang S.-H.,
743 Scadeng M., Saltiel A. R., Olefsky J. M., 2007 Bone marrow|[ndash]|specific Cap gene deletion
744 protects against high-fat diet|[ndash]|induced insulin resistance. Nat. Med. **13**: 455–462.

745 Logan R. W., Robledo R. F., Recla J. M., Philip V. M., Bubier J. A., Jay J. J., Harwood C., Wilcox T., Gatti D.
746 M., Bult C. J., Churchill G. A., Chesler E. J., 2013 High-precision genetic mapping of behavioral traits
747 in the diversity outbred mouse population. Genes, Brain and Behavior **12**: 424–437.

748 Moore J. H., Williams S. M., 2009 Epistasis and Its Implications for Personal Genetics. The American
749 Journal of Human Genetics **85**: 309–320.

750 Motenko H., Neuhauser S. B., O'Keefe M., Richardson J. E., 2015 MouseMine: a new data warehouse
751 for MGI. Mamm Genome **26**: 325–330.

752 Munger S. C., Raghupathy N., Choi K., Simons A. K., 2014 RNA-Seq alignment to individualized
753 genomes improves transcript abundance estimates in multiparent populations. ….

754 Nishikawa S., Yasoshima A., Doi K., Nakayama H., Uetsuka K., 2007 Involvement of sex, strain and age
755 factors in high fat diet-induced obesity in C57BL/6J and BALB/cA mice. Exp. Anim. **56**: 263–272.

756 Ober C., Loisel D. A., Gilad Y., 2008 Sex-specific genetic architecture of human disease. Nature
757 Publishing Group **9**: 911–922.

758 Ordovas J. M., 2006 Genetic interactions with diet influence the risk of cardiovascular disease. Am. J.
759 Clin. Nutr. **83**: 443S–446S.

760 Philip V. M., Sokoloff G., Ackert-Bicknell C. L., Striz M., Branstetter L., Beckmann M. A., Spence J. S.,
761 Jackson B. L., Galloway L. D., Barker P., Wymore A. M., Hunsicker P. R., Durtschi D. C., Shaw G. S.,
762 Shinpock S., Manly K. F., Miller D. R., Donohue K. D., Culiat C. T., Churchill G. A., Lariviere W. R.,
763 Palmer A. A., O'Hara B. F., Voy B. H., Chesler E. J., 2011 Genetic analysis in the Collaborative Cross
764 breeding population. Genome Research **21**: 1223–1238.

765 Philip V. M., Tyler A. L., Carter G. W., 2014 Dissection of complex gene expression using the combined
766 analysis of pleiotropy and epistasis. Pac Symp Biocomput: 200–211.

767 Pierce B. L., Tong L., Chen L. S., Rahaman R., Argos M., Jasmine F., Roy S., Paul-Brutus R., Westra H.-J.,
768 Franke L., Esko T., Zaman R., Islam T., Rahman M., Baron J. A., Kibriya M. G., Ahsan H., 2014
769 Mediation analysis demonstrates that trans-eQTLs are often explained by cis-mediation: a
770 genome-wide analysis among 1,800 South Asians. (JK Pritchard, Ed.). PLoS Genet. **10**: e1004818.

771 Pritchard J. K., Stephens M., Rosenberg N. A., Donnelly P., 2000 Association mapping in structured
772 populations. Am. J. Hum. Genet. **67**: 170–181.

773 R Core Team (2016). R: A language and environment for statistical computing. R Foundation for

774 Statistical Computing, Vienna, Austria. URL https://www.R-project.org/.Avery L., Wasserman S.,
775 1992 Ordering gene function: the interpretation of epistasis in regulatory hierarchies. Trends
776 Genet. **8**: 312–316.

777 Rosenberg N. A., Pritchard J. K., Weber J. L., Cann H. M., Kidd K. K., Zhivotovsky L. A., Feldman M. W.,
778 2002 Genetic structure of human populations. Science **298**: 2381–2385.

779 Schork N. J., 1997 Genetically Complex Cardiovascular Traits. Hypertension **29**: 145–149.

780 Simanski M., Rademacher F., Schröder L., Gläser R., Harder J., 2016 The Inflammasome and the
781 Epidermal Growth Factor Receptor (EGFR) Are Involved in the Staphylococcus aureus-Mediated
782 Induction of IL-1alpha and IL-1beta in Human Keratinocytes (IC Allen, Ed.). PLoS ONE **11**:
783 e0147118.

784 Smith C. L., Goldsmith C.-A. W., Eppig J. T., 2005 The Mammalian Phenotype Ontology as a tool for
785 annotating, analyzing and comparing phenotypic information. Genome Biol. **6**: R7.

786 Svenson K. L., Gatti D. M., Valdar W., Welsh C. E., Cheng R., Chesler E. J., Palmer A. A., McMillan L.,
787 Churchill G. A., 2012 High-resolution genetic mapping using the Mouse Diversity outbred
788 population. Genetics **190**: 437–447.

789 Tyler A. L., Donahue L. R., Churchill G. A., Carter G. W., 2016 Weak Epistasis Generally Stabilizes
790 Phenotypes in a Mouse Intercross (JM Cheverud, Ed.). PLoS Genet. **12**: e1005805–22.

791 Tyler A. L., McGarr T. C., Beyer B. J., Frankel W. N., Carter G. W., 2014 A Genetic Interaction Network
792 Model of a Complex Neurological Disease. Genes, Brain and Behavior.

793 Wang S., Miura M., Jung Y.-K., Zhu H., Li E., Yuan J., 1998 Murine Caspase-11, an ICE-Interacting
794 Protease, Is Essential for the Activation of ICE. Cell **92**: 501–509.

795 Weiss L. A., Pan L., Abney M., Ober C., 2006 The sex-specific genetic architecture of quantitative traits
796 in humans. Nature Genetics **38**: 218–222.

797 Wong A. K., Krishnan A., Yao V., Tadych A., Troyanskaya O. G., 2015 IMP 2.0: a multi-species
798 functional genomics portal for integration, visualization and prediction of protein functions and
799 networks. Nucleic Acids Res. **43**: W128–33.

800 Yalcin B., Wong K., Agam A., Goodson M., Keane T. M., Gan X., Nellåker C., Goodstadt L., Nicod J.,
801 Bhomra A., Hernandez-Pliego P., Whitley H., Cleak J., Dutton R., Janowitz D., Mott R., Adams D. J.,
802 Flint J., 2011 Sequence-based characterization of structural variation in the mouse genome.
803 Nature **477**: 326–329.

804 Yang H., Wang J. R., Didion J. P., Buus R. J., Bell T. A., Welsh C. E., Bonhomme F., Yu A. H.-T., Nachman
805 M. W., Pialek J., Tucker P., Boursot P., McMillan L., Churchill G. A., de Villena F. P.-M., 2011
806 Subspecific origin and haplotype diversity in the laboratory mouse. Nat. Genet. **43**: 648–655.

807